

Increasing hub disruption parallels dementia severity in autosomal dominant Alzheimer disease

Jiaxin Cindy Tu,¹ Peter R. Millar,² Jeremy F. Strain,² Andrew Eck,¹ Babatunde Adeyemo,² Alisha Daniels,² Celeste Karch,³ Edward D. Huey,⁴ Eric McDade,² Gregory S. Day,⁵ Igor Yakushev,⁶ Jason Hassenstab², John Morris,² Jorge J. Llibre-Guerra,² Laura Ibanez,^{2,3,7} Mathias Jucker,^{8,9} Patricio Chrem Mendez,¹⁰ Randell J. Bateman,² Richard J. Perrin,^{2,11} Tammie Benzinger,² Clifford R. Jack Jr,¹² Richard Betzel,¹³ Beau M. Ances,² Adam T. Eggebrecht,¹ Brian A. Gordon,¹ Muriah D. Wheelock,¹ and the Dominantly Inherited Alzheimer Network¹⁴

Abstract

Hub regions in the brain, recognized for their roles in ensuring efficient information transfer, are vulnerable to pathological alterations in neurodegenerative conditions, including Alzheimer Disease (AD). Given their essential role in neural communication, disruptions to these hubs have profound implications for overall brain network integrity and functionality. Hub disruption, or targeted impairment of functional connectivity at the hubs, is recognized in AD patients. Computational models paired with evidence from animal experiments hint at a mechanistic explanation, suggesting that these hubs may be preferentially targeted in neurodegeneration, due to their high neuronal activity levels—a phenomenon termed "activity-dependent degeneration". Yet, two critical issues were unresolved. First, past research hasn't definitively shown whether hub regions face a higher likelihood of impairment (targeted attack) compared to other regions or if impairment likelihood is uniformly distributed (random attack). Second, human studies offering support for activity-dependent explanations remain scarce.

We applied a refined hub disruption index to determine the presence of targeted attacks in AD. Furthermore, we explored potential evidence for activity-dependent degeneration by evaluating if hub vulnerability is better explained by global connectivity or connectivity variations across functional systems, as well as comparing its timing relative to amyloid beta deposition in the brain. Our unique cohort of participants with autosomal dominant Alzheimer Disease (ADAD) allowed us to probe into the preclinical stages of AD to determine the hub disruption timeline in relation to expected symptom emergence.

Our findings reveal a hub disruption pattern in ADAD aligned with targeted attacks, detectable even in pre-clinical stages. Notably, the disruption's severity amplified alongside symptomatic progression. Moreover, since excessive local neuronal activity has been shown to increase amyloid deposition and high connectivity regions show high level of neuronal activity, our observation that hub disruption was primarily tied to regional differences in global connectivity and sequentially followed changes observed in A β PET cortical markers is consistent with the activity-dependent degeneration model. Intriguingly, these disruptions were discernible 8 years before the expected age of symptom onset.

Taken together, our findings not only align with the targeted attack on hubs model but also suggest that activity-dependent degeneration might be the cause of hub vulnerability. This deepened understanding could be instrumental in refining diagnostic techniques and developing targeted therapeutic strategies for AD in the future.

Author affiliations:

¹Department of Radiology, Washington University in St. Louis, St. Louis, MO, USA, 63108

²Department of Neurology, Washington University in St. Louis, St. Louis, MO, USA, 63108

³Department of Psychiatry, Washington University in St. Louis, St. Louis, MO, USA, 63108

⁴Department of Psychiatry and Human Behavior, Warren Alpert Medical School of Brown University, Providence, RI, 02912

⁵Department of Neurology, Mayo Clinic College of Medicine, Jacksonville, FL, USA, 32224

⁶Department of Nuclear Medicine, Technical University of Munich, Munich, Germany, 81675

⁷NeuroGenomics and Informatics Center, Washington University in St. Louis, St. Louis, MO, USA, 63108

⁸Department of Cellular Neurology, Hertie Institute for Clinical Brain Research, University of Tübingen, Tübingen, Germany, 72076

⁹German Center for Neurodegenerative Diseases (DZNE), Tübingen, Germany, 72076

¹⁰Memory Center, Fleni, Argentina, C1428AQK

¹¹Department of Pathology and Immunology, Washington University in St. Louis, St. Louis, MO, USA, 63108

¹²Department of Radiology, Mayo Clinic, Rochester, MN, USA 55905

¹³Department of Psychological and Brain Sciences, Indiana University, Bloomington, IN, USA, 47405

¹⁴A full list of members appears at the end of the manuscript in the Supplementary material

Correspondence to: Muriah Wheelock

Mallinckrodt Institute of Radiology

4525 Scott Ave

St. Louis, MO 63110

mdwheelock@wustl.edu

Running title: Increasing hub disruption parallels dementia severity in autosomal dominant Alzheimer disease

Keywords: neurodegeneration, functional connectivity, hubs, Alzheimer disease, biomarker

Introduction

Alzheimer disease (AD) is the most common neurodegenerative disease that manifests as progressive loss of cognitive functions and affects millions of people worldwide. It is characterized by a cascade of complex pathologic changes in the brain including amyloid beta aggregation and tau tangles, resulting in neurodegeneration¹. While these microscopic changes have been well-documented, there is growing interest in understanding how these pathologies translate to altered brain connectivity patterns observed in AD patients.

Resting-state functional connectivity (FC), as measured with temporal correlations of the blood oxygen level-dependent (BOLD) signals between regions of the brain from fMRI data collected at a task-free state², differs in clinical and pre-clinical AD individuals versus cognitively normal controls^{3–7}. FC is a widely accessible and non-invasive tool for assessing brain organization, and a potential imaging marker for AD^{8–11} since disruptions in connectivity between brain regions may be linked to synaptic changes before cell death and atrophy¹². Prospective imaging studies suggested that the posterior parts of the default mode network deteriorate earlier than anterior parts in AD, providing evidence for a cascading network failure mechanism^{13,14}. Importantly, the initiation of amyloid^{15,16}, and tau¹⁷ pathologies as well as the rate of their accumulation^{18,19} in the brain is not spatially homogenous, providing converging evidence for differences in regional vulnerability to pathological changes. However, precisely what underlies the sequence of regional FC failure, as well as how FC disruptions relate to the molecular pathology is unknown.

Hub regions²⁰ are highly connected nodes with high network centrality that play a critical role in facilitating efficient communication and integration of information across different regions of complex networks. Brain hubs are affected across multiple diseases²¹, including AD^{22,23}. One hypothesis for this hub vulnerability to pathology and degeneration is that hub regions are selectively targeted by activity-dependent damage²⁴. Several lines of evidence support this hypothesis. 1) Hubs have high metabolic demands^{12,25–27}; 2) they are especially susceptible to amyloid beta deposition in AD^{12,27–29}; and, 3) they serve as the spreading centers for tau pathology^{17,30,31}. Due to their topologically central role, targeted attacks on hubs have a more deleterious effect on network efficiency^{21,32–34}. Indeed, FC alterations especially at cortical hubs^{12,23} have been identified in AD patients compared to cognitively normal controls in previous research as well as in mice with extracellular amyloidosis (TgCRND8 mice)³⁵. *In vivo* studies in mice validate the relationship between

neuronal activity level and amyloid-beta deposition^{36,37}, suggesting that increasing amyloid burden through increased baseline activity triggers hub disruptions. While there is strong theoretical and empirical evidence to support the role of hub disruption in AD, little is known concerning the relationship between hub disruption, dementia severity, and symptomatic onset.

Here we leverage a unique population with autosomal dominant AD (ADAD), which allows for accurate estimation of years until symptom onset (EYO) due to the highly predictable onset of cognitive decline³⁸. As a genetic form of the disease, our ADAD participants have a high certainty in AD diagnosis (as opposed to other forms of dementias). Furthermore, since ADAD occurs in a younger population (<60 years) than sporadic AD, we can test associations with AD pathology with minimal confounding co-pathology and can estimate FC network characteristics with minimal age-related changes in neurovascular coupling³⁹.

We examine the regional vulnerability in terms of lower FC by measuring FC hub disruption as a function of ADAD dementia progression from pre-clinical (Clinical Dementia Rating® [CDR®] =0) to moderate and severe dementia (CDR \geq 1). We hypothesize that hub disruption is an early-emerging phenomenon that intensifies with disease progression. Finally, we investigated the relative timing of hub disruption compared to cortical amyloid deposition and cognitive decline. Our goal is to test the targeted attack on hubs model in ADAD over the course of disease progression and obtain evidence for activity-dependent degeneration.

Materials and methods

Participants

Individuals were recruited from the Dominantly Inherited Alzheimer Network (DIAN) Observational Study (<https://dian.wustl.edu/>). Here we examine cross-sectional data from mutation carriers (MC; N = 122) and unaffected non-carriers (NC; N = 85) family members (Supplementary Table 1) with alterations in presenilin 1 (PSEN1), presenilin 2 (PSEN2), or the amyloid precursor proteins (APP)³⁸. Age at symptom onset is relatively consistent within families and mutation types; this allows participants to be staged by their EYO^{38,40}. *Both MCs and NCs have an EYO value based their familial pedigree but only MCs are expected to develop ADAD.* The study was reviewed and approved by the institutional review board at Washington University in St. Louis and written informed consent forms obtained from participants or their legally authorized representatives in accordance with their local institutional review board. The data are from the 15th annual data freeze.

CDR stages

The MCs were further staged by dementia severity using the global Clinical Dementia Rating (CDR(Morris, 1993) into three groups: cognitively normal (CDR = 0), very mild dementia (CDR = 0.5), and mild-to-severe dementia (CDR>=1). To control for the effect of aging, we age-matched the NCs for each MC group according to the following procedure. First, Z-scores were calculated for the age and EYO values separately using their mean and standard deviation across all participants, resulting in a vector of size 2x1 for each participant. The Euclidean distances between the vectors were calculated and the closest MC for each NC participant was determined, defining an age-matched group of NCs for each MC group (Table 1).

MRI Data Acquisition

Neuroimaging protocols have been previously published⁴⁰. Briefly, T1-weighted magnetization-prepared rapid acquisition gradient echo (MP-RAGE) images were acquired at multiple sites on Siemens 3T scanners (Erlangen, Germany). Resting-state fMRI scans were acquired with echo planar imaging (EPI) while participants were instructed to maintain visual fixation on a crosshair. The sequence details are provided in the Supplementary Materials

(Supplementary Table 2). “Pre-scan normalize” was enabled to minimize gain field inhomogeneities attributable to proximity to the receiver coils. Acquisition lasted ~6 minutes each run and the number of acquired runs in the DIAN cohort varied between 1 and 3.

MRI Data Pre-processing

Details on pre-processing followed previously described methods^{6,41} using the 4dfp suite of tools (<http://4dfp.readthedocs.io>). Briefly, slice timing correction and intensity normalization were performed. Head motion was corrected within and across runs. The initial atlas transformation was computed by affine registration of the functional MRI data to an atlas-representative template via the MP-RAGE ($\text{EPI}_{\text{mean}} \rightarrow \text{MP-RAGE} \rightarrow \text{template}$). A final atlas transformation was performed after denoising. Frames with high motion, as measured by DVARS (frame-to-frame signal change over the entire brain) and the frame displacement (FD) measures⁴², were censored. The DVARS criterion was individually set to accommodate baseline shifts (see Supporting Information in⁴³) and the FD criterion was 0.4 mm. Frames were censored if either criterion was exceeded. The time series were band-pass filtered between 0.005 Hz and 0.1 Hz. Censored frames were approximated by linear interpolation for band-pass filtering only and excluded from subsequent steps.

Denoising was then performed with a CompCor-like strategy⁴⁴. As previously described⁴⁵, nuisance regressors were derived from three compartments (white matter, ventricles, and extra-axial space) and were then dimensionality-reduced. White matter and ventricular masks were segmented in each participant using FreeSurfer 5.3⁴⁶ and spatially resampled in register with FC data. The final set of nuisance regressors also included the six parameters derived from rigid body head-motion correction, the global signal averaged over the (FreeSurfer-segmented) brain, and the global signal temporal derivative. Finally, the volumetric time-series were non-linearly warped to Montreal Neurological Institute (MNI) 152 space (3mm)³ voxels using FNIRT⁴⁷.

Functional Connectivity

We selected 246 functional regions of interest (ROIs) separated into 13 networks throughout the cortical and subcortical areas as previously described⁴⁸. The functional ROIs are a combination of cortical ROIs⁴⁹ and subcortical ROIs⁵⁰ (Figure 1A). Regions not reliably covered by the field of view (FOV) such as the cerebellar ROIs were excluded. A list of ROI coordinates and anatomical assignments has been described in previous publications^{41,48} and

can be found in the Supplementary Materials (Supplementary Table 3). FC was estimated using zero-lag Pearson correlations calculated between 246 ROIs and Fisher-Z-transformed to improve normality. The resultant FC matrix can be represented as a graph with nodes as individual ROIs and edges with weights as the correlation values $z(r)$. Group-average FC was generated by averaging the $z(r)$ values across individual FC matrices within each of the CDR and age-matched NC groups (Figure 2).

Data Harmonization

We used Correcting Covariance Batch Effects (CovBat, https://github.com/andy1764/CovBat_Harmonization⁵¹ to remove site effects in mean, variance, and covariance on FC data, with age, mutation, EYO, education, CDR, sex, mutation gene type (PSEN1/PSEN2/APP), and APOE alleles included as the biological covariates that should be protected for during the removal of site effects. After CovBat, two participants (one MC and one NC) were removed from the analysis because they were only represented by a single site and harmonization could not be performed by the CovBat algorithm. The final sample size for analysis was MC = 121 and NC = 84. Similar qualitative results were obtained without the CovBat correction.

Graph Theory Metrics

All graph theory metrics were calculated using the Brain Connectivity Toolbox (BCT, brain-connectivity-toolbox.net), a MATLAB toolbox for complex brain-network analysis⁵². Since regions with a high total positive connectivity tend to have a high total negative connectivity (Supplementary Figure 1), we asymmetrically weighed the positive and negative edges for all measures according to their relative magnitude at a given node following previous literature⁵³. This allows for non-zero strengths at a full FC matrix without threshold (Supplementary Figure 2). Strength is calculated as the sum of signed edge weights around a node in a graph (Figure 1E). This effectively measures global connectivity at an ROI. We also calculated two additional measures of centrality concerning module affiliations⁵⁴: the within-module strength Z-Score (Z) and participation coefficient. Z measures how “well-connected” a node is to other nodes in the module. The participation coefficient measures the diversity of intermodular connections of individual nodes and within-module strength Z-score.

Given that there is no gold standard method for thresholding the FC matrix to create a graph representation and calculate graph metrics^{55,56}, we chose an edge density threshold of

5% for downstream analyses which ensures that the graph is sparse and free of negative correlations⁵⁷. To demonstrate that our results are not dependent on the choice of threshold, we also showed results at a range of edge density similar to previous research⁵⁸, an edge density of 1-5% at 1% intervals and 10%-90% at 10% intervals. This is achieved by finding the maximum spanning tree (MST) backbone first using the BCT toolbox function (backbone_wu.m) and continually adding edges with the largest correlation values until the desired edge density is reached⁵⁹. This is to ensure graph connectedness at the sparsest densities.

Since strength and participation coefficient measures show a correlation with scan time, the remaining scan time after frame censoring was regressed out of these graph metrics to correct for the possible confound of individual differences in total scan time remaining after frame censoring (Supplementary Figure 3).

Hub Disruption Index

To measure how the centrality of each region differs from a healthy reference, we chose NC match 1 to be the reference group. This choice is motivated by the fact that this group is the closest to what is usually considered young, healthy adults^{22,23}, which has been used as a baseline for calculating hub disruption in prior studies²³. The average nodal FC strength of the NC match 1 group was calculated and the percentage difference from this baseline average strength was calculated for each MC group (CDR = 0, CDR = 0.5, CDR \geq 1; Figure 3B) and the remaining two NC groups (NC match 2, NC match 3). While using a consistent baseline reference group enables comparison of the metric across groups⁶⁰, we also ran a supplementary analysis using the age-matched NC groups as a reference for each MC group and obtained qualitatively the same result.

We calculated a normalized hub disruption index adapted from prior work⁶⁰ by fitting a linear regression slope (κ_S) where the dependent variable is the difference in strength for either the group average or an individual from the average strength of the reference group, which is then normalized by dividing the average strength of the reference group. The primary method by which selective hub disruption has been indexed in prior work is to calculate the slope of the linear regression model between the mean local network measures of a reference group, and the difference between that reference and the participant under study^{23,60-63} (Figure 1A). A negative slope has been interpreted as the presence of hub disruption. In practice, this definition has difficulty distinguishing between a targeted attacks

on network hubs vs. a random attack, as the correlation would appear negative under both models. An intuitive analogy is to examine the effect of a natural disaster on the affluent or impoverished areas. While affluent areas of a city lose more in absolute amounts, it is unclear whether they are *disproportionally more* affected, or it is merely an effect of starting from a higher baseline point. We, therefore, modified the “hub disruption index” to measure the *percentage* difference in connectivity strength versus baseline connectivity strength such that only targeted attacks on hubs would result in a negative linear regression slope (Figure 1B). We also standardized the baseline strength into Z-scores to increase the interpretability of the metric. In this way, we can unambiguously test the selective reduction in global connectivity at hubs and compare the hub disruption index quantitatively across disease stages. The mathematical equation is shown below:

$$\frac{\text{strength}_{\text{test}} - \langle \text{strength}_{\text{ref}} \rangle}{\langle \text{strength}_{\text{ref}} \rangle} * 100 = \text{zscore}(\langle \text{strength}_{\text{ref}} \rangle) \quad (1)$$

A more negative hub disruption index here indicates that the strengths in high-strength hubs are reduced by a larger proportion than in other low-strength regions, whereas a zero-hub disruption index indicates that the strength in high-strength regions and low-strength regions are changed to the same extent.

We used global connectivity strength as the primary measure of centrality due to its simplicity and strong correspondence to other measures in AD disease factors, e.g. hubs with high global FC have spatial correspondence with amyloid deposition^{16,18,28}, tau burdens³⁰ and metabolic factors^{26,64}. However, there exist alternative definitions for hubs^{20,57,65}. Specifically, some researchers argued that in functional networks, the participation coefficient, which captures the diversity of connections to different modules, is the key metric for regional importance or centrality⁵⁷. On the other hand, within-module strength Z score is also an important measure of nodal centrality⁵⁴. Therefore, we additionally examined hub disruption as defined by the participation coefficient and within-module Z-score using a similar asymmetric weighting⁵³ with the BCT toolbox functions (participation_coef_sign.m) and custom MATLAB scripts, respectively.

Cognitive Composite Score

We used a cognitive composite score (CCS)⁶⁶⁻⁶⁸, developed for use as an outcome measure in DIAN clinical trials, to measure the cognitive decline for each individual. CCS is a global summary of cognitive functions. Details of the calculation have been previously

described⁶⁸. Briefly, a cognitive composite score is calculated by averaging each test's normalized scores by equal weight for 1) the DIAN Word List test delayed recall, 2) the delayed recall score from the Wechsler Memory Scale-Revised Logical Memory IIA subtest, 3) the Mini-Mental State Exam (MMSE), and 4) the Wechsler Adult Intelligence Scale-Revised Digit-Symbol Substitution test (Supplementary Table 4). Normalization was carried out with respect to the mean and SD reported in a population sample of 58 MCs with EYO \leq 15⁶⁸. For analyses using the cognitive composite scores, we excluded one MC with a >1 year gap between psychometric tests and MRI sessions, and additionally 9 MC who did not complete all four tests.

Positron emission tomography (PET) measures of cortical amyloid deposition

Amyloid-beta PET imaging with Pittsburgh Compound B (PiB) was performed using a bolus injection of [11C] PiB⁴⁰. PET data were acquired using either a 70-min scan beginning at the start of the injection or a 30-min scan starting 40 min after the injection. Data were converted to regional standardized uptake value ratios (SUVRs) relative to the cerebellar grey matter using ROI generated in FreeSurfer⁴⁶ with partial volume correction via a regional spread function. Amyloid positivity was defined as PiB partial volume corrected SUVR across the precuneus, prefrontal, gyrus rectus, and temporal FreeSurfer regions of interest (ROI) >1.42 ^{69,70}.

Statistical Models for Biomarkers

Generalized Additive Mixed Models were fit with the *gamm()* function from R package (*mgcv*) to examine the relationship between different biomarkers and the EYO. A smooth function was applied to the EYO separated by mutation carrier status (MC or NC), with sex, education as fixed effect covariates, and a random effect of family. The time of divergence between MC and NC was determined as the point where the predicted 95% simultaneous confidence interval starts to have no overlap⁷¹. For predicting the response of κ_S , we further include the residual motion measure (DVARS) as a covariate.

For the relationship between CCS and κ_S , we fit a linear mixed effects model with fixed effect covariates sex, education, DVARS and age and a random effect of family with the *lmer()* function from R package *lme4*.

Statistical Tests and Visualization

All standard statistical tests (e.g., F-tests, t-tests, ANOVA) were performed with MATLAB R2020b or R (4.1.0). FDR⁷² was used for the correction of multiple comparisons at a significance level of 0.05.

Visualizations of regional graph theory metrics on the brain and FC matrix were generated using Network Level Analysis toolbox (Beta version) (<https://github.com/mwheelock/Network-Level-Analysis>), BrainNet Viewer toolbox⁷³, and custom MATLAB and R scripts.

Data availability

Data that support the findings of this study are available from DIAN at <https://dian.wustl.edu/our-research/observational-study/dian-observational-study-investigator-resources/>.

Results

MC and NC groups do not differ in demographic features and data quality

As designed, each of the MC and NC-matched CDR groups did not differ in age or EYO (Table 1). The matched groups also did not differ in DVARS or minutes of low-motion data. Not surprisingly, the CDR 0 groups did not differ on CCS, however, the MC and NC groups differed on CCS at CDR = 0.5 and CDR \geq 1.

A selected subset of ROIs shows significant differences in strength from the healthy reference

We defined the average strength of ROIs in the young cognitively normal non-carrier group (NC match 1, N = 52) as a reference of hub centrality (Figure 3A). We first established that the number of participants and minutes of FC data were sufficient to obtain reliable group-level RSFC measures (Appendix A). Notably, we were able to identify the hubs described in literature^{28,58,74}, e.g. precuneus/posterior cingulate, dorsolateral prefrontal

cortex, supramarginal gyrus, medial prefrontal cortex (Figure 3A; Supplementary Figure 4). This is robust to the choice of edge density threshold and

and/or percentile cut-offs (Supplementary Figure 5). Additionally, we compared the ROI strengths between all MC groups and the reference using a two-sample t-test (FDR<0.05) (Supplementary Figure 6). Briefly, no ROI had significant difference in strength between MC (CDR=0) and the reference. In MC (CDR=0.5), 19 ROIs covering the superior frontal gyrus, precuneus, middle temporal gyrus, middle occipital gyrus, middle frontal gyrus, inferior parietal lobule, inferior occipital gyrus, fusiform gyrus and cuneus have significantly lower strength compared to the reference. In MC (CDR≥1), three ROIs (in the insula, thalamus and parahippocampal gyrus) showed significant higher strength compared to the reference, and 30 ROIs (in angular gyrus, anterior cingulate, claustrum, cuneus, fusiform gyrus, inferior parietal lobule, inferior temporal gyrus, insula, medial frontal gyrus, middle occipital gyrus, middle temporal gyrus, parahippocampal gyrus, postcentral gyrus, posterior cingulate, precuneus, superior frontal gyrus, superior temporal gyrus and thalamus) showed significantly lower strength compared to the reference. On the other hand, none of the ROIs in NC match 2 or NC match 3 groups shown significant differences in strength from NC match 1 (Supplementary Figure 7).

Hub disruption increases with CDR stage, not age

We measured the group-level hub disruption index by calculating the percentage difference from the reference for the mean strength in each of the MC groups (CDR=0, CDR=0.5, and CDR ≥ 1) (Figure 3B; Supplementary Figure 8). The group-level hub disruption index for all three MC CDR groups was significantly different from zero (Table 2). In addition, κ_S became increasingly more negative across CDR stages. The hub disruption index (a.k.a. regression slope in Figure 3B) is significantly different between MC (CDR = 0.5) and MC (CDR = 0) ($F(1,488) = 12.0$, $P<0.001$, partial $\eta^2 = 0.024$), between MC (CDR=0.5) and MC (CDR≥1) ($F(1,488) = 22.6$, $P<0.001$, partial $\eta^2 = 0.044$), and between MC (CDR=0) and MC (CDR≥1) ($F(1,488) = 61.6$, $P<0.001$, partial $\eta^2 = 0.112$). Our results are qualitatively replicated at a wide range of threshold choices (Supplementary Figure 9). On average, nodes in the cingulo-opercular network showed the highest baseline strength and largest % strength difference from baseline across multiple thresholds (Supplementary Figure 10). In addition to the group-level hub disruption index, we calculated the hub disruption index for each participant in the MC and NC groups. All MC groups had a hub disruption

index that differed from zero (FDR-adjusted $P<0.001$) while no NC group had a hub disruption index that differed from zero (FDR-adjusted $P>0.05$) (Supplementary Figure 11, Supplementary Table. 5). Specifically, for MC, a one-way ANOVA demonstrated that the hub disruption index differed across the CDR groups ($F(2,118) = 8.8$, $P<0.001$, $\eta^2 = 0.130$). Post-hoc two-sample t-tests with FDR correction revealed significant group differences ($t(87) = 4.03$, $P = 0.002$, Cohen's $d = 1.02$) between CDR=0 ($M = -5.6$, $SD = 11.1$) and CDR ≥ 1 participants ($M = -16.7$, $SD = 10.3$), and between CDR=0.5 ($M = -9.6$, $SD = 9.6$) and CDR ≥ 1 participants ($t(50) = 2.52$, $P = 0.03$, Cohen's $d = 0.72$) (Figure 3C).

Next, we asked whether this observation can be explained by increasing age. We calculated the hub disruption index for the age-matched NC groups 2 and 3 with the same procedure (Figure 3D). The group-level hub disruption index for NC groups did not significantly differ from zero (Table 2). At the individual level, there were no differences among NC groups (one-way ANOVA, $F(2,81) = 0.07$, $P = 0.93$) (Figure 3E), nor a significant relationship between κ_s and age in NC (linear regression, $\beta = 0.01$, $R^2 < 0.001$, $F(2,82) = 0.0072$, $P = 0.933$).

Changes in AD biomarkers often precedes dementia symptoms in AD^{38,75,76}. A subset of the MC (CDR=0) group can be classified as amyloid beta positive (A β +) ($N = 29/60$) according to their amyloid PET results (Methods). With one-sample t-tests with FDR correction, we found that both groups had hub disruption index significantly lower than 0 (A β -: $M = -5.4$, $SD = 11.2$, Cohen's $d = -0.48$, $t(30) = -2.7$, $P = 0.012$; A β +: $M = -5.7$, $SD = 11.5$, Cohen's $d = -0.50$, $t(28) = -2.6$, $P = 0.012$). However, there was no significant difference in hub disruption index between the A β - and A β + groups (two-sample t-test, two-tailed $P = 0.92$) (Figure 3F-G). Changes in amyloid-beta accumulation in PET imaging often precedes dementia symptoms in AD^{38,75,76}. A subset of the MC (CDR=0) group can be classified as amyloid beta positive (A β +) ($N = 29$) according to their amyloid PET results (Methods). With one-sample t-tests with FDR correction, we found that both groups have hub disruption index significantly lower than 0 (A β -: $M = -5.4$, $SD = 11.2$, Cohen's $d = -0.48$, $t(30) = -2.7$, $P = 0.012$; A β +: $M = -5.7$, $SD = 11.5$, Cohen's $d = -0.50$, $t(28) = -2.6$, $P = 0.012$). However, there was no significant difference in hub disruption index between the A β - and A β + groups (two-sample t-test, two-tailed $P = 0.92$) (Figure 3F-G).

Hub disruption is best explained by differences in regional global connectivity

To understand the key drivers of hub vulnerability in ADAD, we calculated the hub disruption index using two alternative measures based on their network membership instead of global connectivity strength: 1) the within-module connectivity rank (within-module strength Z-score, Z) and 2) the connectivity diversity (Participation Coefficient, P_c) (Figure 4A). Overall, both participation coefficient and within module Z-score effects were less sensitive to ADAD progression than using the global connectivity strength as the reference. Thus, we focused subsequent analyses on the hub disruption index with regards to the global connectivity strength. Detailed statistics can be found in Table 2 and Appendix B.

Hub disruption index diverges between mutation carriers and non-carriers at an earlier EYO than the separation of general cognitive performance

Generalized Additive Mixed Models were fit to examine the relationship between hub disruption or other biomarkers and the EYO, as well as to obtain the point of divergence between MC and NC. For the hub disruption index (κ_S), this was calculated to be $EYO = -7.9$ years (Figure 5A). In comparison, the total cortical amyloid deposition measured as PiB SUVR ratio diverged at $EYO = -14.8$ (Figure 5B), and the cognitive composite score measure diverged at $EYO = -6.8$ years (Figure 5C). Thus, we found that the divergence of hub disruption index preceded the divergence of cognitive performance measure and followed the earlier stage of amyloid deposition.

Greater hub disruption is correlated with worse general cognition

Lastly, we found there existed a positive correlation between κ_S and CCS ($r=0.3$, $t(110)=3.27$, $P=0.001$). We further examined whether an individual's hub disruption could explain unique variance in the cognitive composite score of individual MCs after controlling for potentially confounding covariates (age, sex, years of education, motion in scan measured by DVARS; and family as a random effect. The hub disruption index was positively related with cognitive composite scores at the edge threshold of 5% ($\beta_{\kappa_S}=0.02\pm0.01$, $t(105)=2.53$, $P=0.013$) and across different edge thresholds (Table 3, Figure 5D), suggesting that greater

hub disruption (a.k.a. more negative hub disruption index) correlated with worse general cognition.

Discussion

Consistent with a targeted attack on hubs model, the proportion of reduction in FC at individual regions in ADAD was positively related to the total global connectivity of that region in the unaffected family members of ADAD participants. This preferential disruption of hub connectivity increased with CDR stage but not age, is best explained by global connectivity, less so to the within-module connectivity rank, and not to the diversity of connectivity across resting-state networks. This preferential disruption of hub connectivity is seen at all stages of disease progression in ADAD MC and starts to differentiate MC and NC at about EYO = 8 years. Additionally, greater (more negative) hub disruption was associated with worse general cognition after controlling for relevant covariates.

Progressive hub disruption is consistent with popular network failure models of AD

Prior studies endorse a cascading network failure starting from the posterior default mode network (DMN) and progressing to the anterior and ventral DMN¹³. Our results complement this observation by providing a possible underlying mechanism for this cascading process and extending it beyond default mode network, whereby the vulnerability of regions to the reduction in FC is dependent on their centrality in the whole brain network. Nodes that have the highest centrality (e.g., posterior default mode network, Figure 3A) were among the first to show decreased FC, consistent with existing literature¹³. Over time, changes in processing burden shifts from one hub to other hubs, further enhancing the aberrant amyloid- β precursor protein processing and amyloidosis in the other hubs¹³, consistent with our progressive increase in hub disruption with disease. Admittedly, FC is an indirect measure of connectivity across regions, and future research could investigate hub vulnerability in structural networks using diffusion MRI.

Hub disruption is best explained by global connectivity

Despite the wide use of “functional hubs” in the literature, what defines a functional hub has not reached a consensus^{20,57,65}. Hubs can be described in terms of their network membership (e.g., default mode network), where connectors are important for communication between networks and module centers are important for communication within networks. The nodes with high abundance of intermodule connections (connectors) form a structural rich club⁸⁰, which are also known to be affected in AD⁸¹, although this concept is not universally accepted (other studies suggest that the highly rich-club core was preserved and the disruptions started in the periphery⁸²). Previous literature on brain lesion patients suggested that the integrity of brain network organization is severely compromised when damage is in connectors but not module centers⁸³. Other studies also report differential outcomes in network structure when damage is localized to module centers or connectors³⁴. One recent study has also suggested that the amyloid-beta accumulation rate was faster at connectors¹⁹. On the other hand, our results here suggested that hub disruption is best explained by differences in global connectivity across regions, rather than their roles to communicate between or within networks. This is in line with the hypothesis that high metabolic demands associated with high global connectivity may trigger downstream cellular and molecular events that result in neurodegeneration¹³, conveying preferential/selective vulnerability. For example, calcium instability caused by amyloid beta peptides may render human cortical neurons vulnerable to excitotoxicity⁸⁴, and this could result in further neurodegeneration in AD⁸⁵.

Hub disruption predates cognitive changes but follows amyloid PET changes

The effectiveness of a biomarker can be evaluated based on its ability to detect early indications of pathology prior to disease onset. Investigating the initial stages of decline in healthy brains compared to those AD offers substantial potential for early identification before AD symptoms manifest. Because of the highly consistent familial disease onset for ADAD, we were able to compare this biomarker across EYO and other disease-related changes including cognitive composite scores and cortical amyloid deposition. We found that the hub disruption index first demonstrated a divergence between groups ~8 years before EYO—much earlier than the divergence in global FC signature (~4 years)—between converters and non-converters in sporadic AD⁷¹. Hub disruption index also diverges between MCs and NCs before the changes in the general cognitive score (~7 years), but after hypo-

metabolism (~10 year), and increased concentrations of cerebral spinal fluid tau protein (~15 year)³⁸, and the amyloid PET changes (~15 year). This is consistent with previously hypothesized disease progression where the FC disruption follows from amyloid-beta deposition and potentially excessive chronic activity^{24,86}, and eventually contributes to cognitive impairment (Supplementary Figure 16). We did not find significant differences between the hub disruption index in A β + and A β - participants in the MC (CDR=0) group, despite A β + participants having slightly negative hub disruption index. However, this lack of a difference between A β - and A β + individuals should be viewed cautiously given the modest sample sizes. We do note the limitation that our EYO calculation is based on mutation and parental symptom onset and may not precisely reflect the true EYO. Therefore, the best practice is to interpret the EYO years in relative terms for different biomarkers instead of taking it at purely its face value. We did not find significant differences between the hub disruption index in A β + and A β - participants in the MC (CDR=0) group, despite A β + participants having slightly negative hub disruption index. However, this lack of a difference between A β - and A β + individuals should be viewed cautiously given the small sample size for the comparison.

Comparison to other network topology studies in AD

Other studies of network topology in AD have examined global graph theory measures such as small-worldness, global clustering coefficient, and characteristic path length^{58,87}. However, those measures are generally sensitive to network sparsity and require a careful choice of null models⁸⁸. Further, it is hard to interpret the biological relevance for those global measures. In contrast, hubs with high global FC have been linked to amyloid deposition^{16,18,28}, tau burden³⁰ and metabolic factors^{26,64}. They also overlap with the regions that demonstrated high heritability⁸⁹. Therefore, our research on hub vulnerability is literature-driven with an attempt to link abstract network topology measures to molecular and cellular pathologies.

Implications for AD research, prevention, and treatment

We found that hub disruption, or increased vulnerability to reduced FC at highly central hub regions, is prevalent across the course of ADAD, with increasing severity as the disease progresses. Our results here have key implications for future AD research and therapeutics development: we provided a testable hypothesis where targeted pharmacological

manipulation, non-invasive stimulation, or behavioral training to alter neuronal excitability⁹⁰ especially at hub regions could alter the progression of AD. Existing research has demonstrated in an awake rodent model that acute inactivation of a hub region (dorsal anterior cingulate cortex) has profound effects on the whole network⁹¹. Future studies in animal models of AD could further validate this with optogenetic and chemogenetic manipulations. Furthermore, previous literature has suggested that “restoration of the topology of resting-state FC may aid in cognitive repair and recovery”^{32,92}, and those can be further tested in future studies.

On the other hand, we found that hub disruption is positively related to the cognitive composite scores after considering the effect of age, sex, years of education, and average motion of retained frame. And the separation of hub disruption between MC and NC starts shortly after the increased levels of cortical amyloid deposition and at around the same time as preclinical measures of cognitive decline. This indicates that our new measure of resting-state FC change has the potential to act as a non-invasive, low-cost, and accessible biomarker especially given compared to CSF and PET for prevention studies and clinical trials to aid the development of new treatments and monitor their effectiveness. Other biomarkers focusing on DMN network failure have been proposed⁹³, but our measure is conceptually straightforward, easy to calculate, and biologically intuitive. In addition, previous measures have focused on distinguishing AD patients from controls, whereas the current study mapped a progressive relationship between FC and centrality across the clinical dementia stages.

Limitations and future directions

While we concluded that increasing hub disruption was related to disease progression and not aging, participants involved in this study were relatively young (18-69 years). It is still possible that a similar increase in hub vulnerability would be observed at a much older age, as seen in other age-related changes in FC^{94,95}. Notably, another study using cognitively normal adults from OASIS-3 (42-95 years) seemed to show the opposite result to the current study¹⁹, whereby functional hubs were particularly vulnerable to the higher annual accumulation of amyloid beta but have a slower FC decrease than non-hub regions. However, there are also several important methodological differences between that study and ours: 1) they employed the GLASSO algorithm to estimate FC with only direct connections while we used the simple Pearson’s correlation, and 2) they define hubs as regions with high participation coefficients and we found that at certain edge density threshold, the strength and

the participation coefficient of a node could be negatively correlated. Additionally, even though previous work has found comparable FC changes in ADAD to sporadic AD (Smith et al., 2021; Strain et al., 2022; Wheelock et al., 2023), our results are yet to be confirmed in sporadic AD. Further validations on longitudinal changes, and on subjects with more imaging data are needed to assess whether hub disruption could be a reliable biomarker of individual disease progression in AD. Furthermore, future investigations in large brain-wide single-cell transcriptome data (e.g. Allen Human Brain Atlas) may be useful in linking the hub vulnerability to the underlying biological mechanisms^{96,97}.

Conclusions

We investigated the relationship between FC differences across ROIs and baseline centrality measures. We demonstrated that hubs with high global connectivity are especially vulnerable to reduction in FC in individuals with ADAD, consistent with a targeted attack on hubs model. Moreover, this disruption of hub connectivity becomes more severe with increasing CDR stage and occurs around 8 years before symptom onset, slightly preceding cognitive changes but following amyloid PET changes, indicating the early and progressive nature of hub vulnerability in AD. Interestingly, our results also suggest that the preferential disruption of FC in hub regions is more related to global connectivity rather than within-module connectivity or diversity of connectivity across networks. These findings provide insights into the complex dynamics of brain network dysfunction in AD and the critical role of hubs in this process.

Acknowledgements

Data collection and sharing for this project was supported by The Dominantly Inherited Alzheimer Network (DIAN, U19AG032438) funded by the National Institute on Aging (NIA), the Alzheimer's Association (SG-20-690363-DIAN), the German Center for Neurodegenerative Diseases (DZNE), Raul Carrea Institute for Neurological Research (FLENI), Partial support by the Research and Development Grants for Dementia from Japan Agency for Medical Research and Development, AMED, and the Korea Health Technology R&D Project through the Korea Health Industry Development Institute (KHIDI), Spanish Institute of Health Carlos III (ISCIII), Canadian Institutes of Health Research (CIHR), Canadian Consortium of Neurodegeneration and Aging, Brain Canada Foundation, and Fonds

de Recherche du Québec – Santé. This manuscript has been reviewed by DIAN Study investigators for scientific content and consistency of data interpretation with previous DIAN Study publications. We acknowledge the altruism of the participants and their families and contributions of the DIAN research and support staff at each of the participating sites for their contributions to this study.

During the preparation of this work the author(s) used ChatGPT in order to increase the clarity and conciseness of the language. After using this tool/service, the author reviewed and edited the content as needed and take full responsibility for the content of the publication.

We would like to additionally thank Aaron Tanenbaum for processing the MRI data, Dr. Julie Wisch and Dr. Tyler Blazey and Dr. Matt Welhaf for their suggestions and assistance in estimating the divergence of metrics between mutation carriers and non-carriers, as well as Dr. Nilanjan Chakraborty, Sayan Das, Dr. Aishwarya Rajesh, and Jiaqi Li for their discussion on the mathematical rigor.

Funding

This study is supported by the Administrative Supplement to K99 EB029343 to M.D.W and CCSN fellowship by the McDonnell Center for Systems Neuroscience to J.C.T. Additional support for this study was provided by NIH grants: R00EB029343, K01 AG053474, P30 NS098577, P30 AG066444 Research Education Component, National Science Foundation (DGE-1745038), the National Institute for Health Research (NIHR) Queen Square Dementia Biomedical Research Centre, and the Medical Research Council Dementias Platform UK (MR/L023784/1 and MR/009076/1). Daniel J Brennan MD Fund and the Paula and Rodger Riney Fund.

Competing interests

All authors report no competing interests.

Supplementary material

Supplementary material is available at *Brain* online

Appendix 1

Dominantly Inherited Alzheimer Network

Randall Bateman, Alisha J. Daniels, Laura Courtney, Eric McDade, Jorge J. Libre-Guerra, Charlene Supnet-Bell, Chengie Xiong, Xiong Xu, Ruijin Lu, Guoqiao Wang, Yan Li, Emily Gremminger, Richard J. Perrin, Erin Franklin, Laura Ibanez, Gina Jerome, Elizabeth Herries, Jennifer Stauber, Bryce Baker, Matthew Minton, Carlos Cruchaga, Alison M. Goate, Alan E. Renton, Danielle M. Picarello, Tammie Benzinger, Brian A. Gordon, Russall Hornbeck, Jason Hassenstab, Jennifer Smith, Sarah Stout, Andrew J. Aschenbrenner, Celeste M. Karch, Jacob Marsh, John C. Morris, David M. Holtzman, Nicolas Barthelemy, Jinbin Xu, James M. Noble, Sarah B. Berman, Snezana Ikonomovic, Neelesh K. Nadkarni, Gregory S. Day, Neill R. Graff-Radford, Martin Farlow, Jasmeer P. Chhatwal, Takeshi Ikeuchi, Kensaku Kasuga, Yoshiki Niimi, Edward D. Huey, Stephen Salloway, Peter R. Schofield, William S. Brooks, Jacob A. Bechara, Ralph Martins, Nick C. Fox, David M. Cash, Natalie S. Ryan, Mathias Jucker, Christoph Laske, Anna Hofmann, Elke Kuder-Buleta, Susanne Graber-Sultan, Ulrike Obermueller, Johannes Levin, Yvonne Roedenbeck, Jonathan Vöglein, Jae-Hong Lee, Jee Hoon Roh, Raquel Sanchez-Valle, Pedro Rosa-Neto, Ricardo F. Allegri, Patricio Chrem Mendez, Ezequiel Surace, Silvia Vazquez, Francisco Lopera, Yudy Milena Leon, Laura Ramirez, David Aguillon, Allan I. Levey, Erik C.B Johnson, Nicholas T. Seyfried, John Ringman, Anne M. Fagan, and Hiroshi Mori.

References

1. Musiek ES, Holtzman DM. Three dimensions of the amyloid hypothesis: time, space and “wingmen.” *Nat Neurosci.* 2015;18(6):800-806. doi:10.1038/nn.4018
2. Biswal B, Zerrin Yetkin F, Haughton VM, Hyde JS. Functional connectivity in the motor cortex of resting human brain using echo-planar mri. *Magnetic Resonance in Medicine.* 1995;34(4):537-541. doi:10.1002/mrm.1910340409
3. Chhatwal JP, Schultz AP, Johnson K, et al. Impaired default network functional connectivity in autosomal dominant Alzheimer disease. *Neurology.* 2013;81(8):736-744. doi:10.1212/WNL.0b013e3182a1aafe
4. Dennis EL, Thompson PM. Functional Brain Connectivity Using fMRI in Aging and Alzheimer’s Disease. *Neuropsychol Rev.* 2014;24(1):49-62. doi:10.1007/s11065-014-9249-6

5. Sheline YI, Raichle ME. Resting State Functional Connectivity in Preclinical Alzheimer's Disease. *Biological Psychiatry*. 2013;74(5):340-347. doi:10.1016/j.biopsych.2012.11.028
6. Smith RX, Strain JF, Tanenbaum A, et al. Resting-State Functional Connectivity Disruption as a Pathological Biomarker in Autosomal Dominant Alzheimer Disease. *Brain Connectivity*. 2021;11(3):239-249. doi:10.1089/brain.2020.0808
7. Yu M, Sporns O, Saykin AJ. The human connectome in Alzheimer disease — relationship to biomarkers and genetics. *Nat Rev Neurol*. 2021;17(9):545-563. doi:10.1038/s41582-021-00529-1
8. Thomas JB, Brier MR, Bateman RJ, et al. Functional Connectivity in Autosomal Dominant and Late-Onset Alzheimer Disease. *JAMA Neurology*. 2014;71(9):1111-1122. doi:10.1001/jamaneurol.2014.1654
9. Dickerson BC, Sperling RA. Neuroimaging Biomarkers for Clinical Trials of Disease-Modifying Therapies in Alzheimer's Disease. *NeuroRX*. 2005;2(2):348-360. doi:10.1602/neurrx.2.2.348
10. Sorg C, Riedl V, Perneczky R, Kurz A, Wohlschlager AM. Impact of Alzheimer's Disease on the Functional Connectivity of Spontaneous Brain Activity. *Current Alzheimer Research*. 2009;6(6):541-553. doi:10.2174/156720509790147106
11. Buckley RF, Schultz AP, Hedden T, et al. Functional network integrity presages cognitive decline in preclinical Alzheimer disease. *Neurology*. 2017;89(1):29-37. doi:10.1212/WNL.0000000000004059
12. Drzezga A, Becker JA, Van Dijk KRA, et al. Neuronal dysfunction and disconnection of cortical hubs in non-demented subjects with elevated amyloid burden. *Brain*. 2011;134(Pt 6):1635-1646. doi:10.1093/brain/awr066
13. Jones DT, Knopman DS, Gunter JL, et al. Cascading network failure across the Alzheimer's disease spectrum. *Brain*. 2016;139(2):547-562. doi:10.1093/brain/awv338
14. Jones DT, Graff-Radford J, Lowe VJ, et al. Tau, amyloid, and cascading network failure across the Alzheimer's disease spectrum. *Cortex*. 2017;97:143-159. doi:10.1016/j.cortex.2017.09.018
15. Gordon BA, Blazey TM, Su Y, et al. Spatial patterns of neuroimaging biomarker change in individuals from families with autosomal dominant Alzheimer's disease: a longitudinal study. *The Lancet Neurology*. 2018;17(3):241-250. doi:10.1016/S1474-4422(18)30028-0
16. Palmqvist S, Schöll M, Strandberg O, et al. Earliest accumulation of β -amyloid occurs within the default-mode network and concurrently affects brain connectivity. *Nat Commun*. 2017;8(1):1214. doi:10.1038/s41467-017-01150-x
17. Frontzkowski L, Ewers M, Brendel M, et al. Earlier Alzheimer's disease onset is associated with tau pathology in brain hub regions and facilitated tau spreading. *Nat Commun*. 2022;13(1):4899. doi:10.1038/s41467-022-32592-7

18. Villain N, Chételat G, Grassiot B, et al. Regional dynamics of amyloid- β deposition in healthy elderly, mild cognitive impairment and Alzheimer's disease: a voxelwise PiB-PET longitudinal study. *Brain*. 2012;135(7):2126-2139. doi:10.1093/brain/aws125
19. Liu G, Shen C, Qiu A. Amyloid- β accumulation in relation to functional connectivity in aging: A longitudinal study. *NeuroImage*. 2023;275:120146. doi:10.1016/j.neuroimage.2023.120146
20. van den Heuvel MP, Sporns O. Network hubs in the human brain. *Trends in Cognitive Sciences*. 2013;17(12):683-696. doi:10.1016/j.tics.2013.09.012
21. Crossley NA, Mechelli A, Scott J, et al. The hubs of the human connectome are generally implicated in the anatomy of brain disorders. *Brain*. 2014;137(8):2382-2395. doi:10.1093/brain/awu132
22. Dai Z, Yan C, Li K, et al. Identifying and Mapping Connectivity Patterns of Brain Network Hubs in Alzheimer's Disease. *Cerebral Cortex*. 2015;25(10):3723-3742. doi:10.1093/cercor/bhu246
23. Yu M, Engels MMA, Hillebrand A, et al. Selective impairment of hippocampus and posterior hub areas in Alzheimer's disease: an MEG-based multiplex network study. *Brain*. 2017;140(5):1466-1485. doi:10.1093/brain/awx050
24. de Haan W, Mott K, Straaten ECW van, Scheltens P, Stam CJ. Activity Dependent Degeneration Explains Hub Vulnerability in Alzheimer's Disease. *PLOS Computational Biology*. 2012;8(8):e1002582. doi:10.1371/journal.pcbi.1002582
25. Tomasi D, Wang GJ, Volkow ND. Energetic cost of brain functional connectivity. *Proceedings of the National Academy of Sciences*. 2013;110(33):13642-13647. doi:10.1073/pnas.1303346110
26. Vaishnavi SN, Vlassenko AG, Rundle MM, Snyder AZ, Mintun MA, Raichle ME. Regional aerobic glycolysis in the human brain. *Proceedings of the National Academy of Sciences*. 2010;107(41):17757-17762. doi:10.1073/pnas.1010459107
27. Bullmore E, Sporns O. The economy of brain network organization. *Nat Rev Neurosci*. 2012;13(5):336-349. doi:10.1038/nrn3214
28. Buckner RL, Sepulcre J, Talukdar T, et al. Cortical Hubs Revealed by Intrinsic Functional Connectivity: Mapping, Assessment of Stability, and Relation to Alzheimer's Disease. *J Neurosci*. 2009;29(6):1860-1873. doi:10.1523/JNEUROSCI.5062-08.2009
29. Myers N, Pasquini L, Göttler J, et al. Within-patient correspondence of amyloid- β and intrinsic network connectivity in Alzheimer's disease. *Brain*. 2014;137(7):2052-2064. doi:10.1093/brain/awu103
30. Cope TE, Rittman T, Borchert RJ, et al. Tau burden and the functional connectome in Alzheimer's disease and progressive supranuclear palsy. *Brain*. 2018;141(2):550-567. doi:10.1093/brain/awx347

31. Franzmeier N, Neitzel J, Rubinski A, et al. Functional brain architecture is associated with the rate of tau accumulation in Alzheimer's disease. *Nat Commun.* 2020;11(1):347. doi:10.1038/s41467-019-14159-1
32. Alstott J, Breakspear M, Hagmann P, Cammoun L, Sporns O. Modeling the Impact of Lesions in the Human Brain. *PLOS Computational Biology.* 2009;5(6):e1000408. doi:10.1371/journal.pcbi.1000408
33. Achard S, Salvador R, Whitcher B, Suckling J, Bullmore E. A Resilient, Low-Frequency, Small-World Human Brain Functional Network with Highly Connected Association Cortical Hubs. *J Neurosci.* 2006;26(1):63-72. doi:10.1523/JNEUROSCI.3874-05.2006
34. Honey CJ, Sporns O. Dynamical consequences of lesions in cortical networks. *Human Brain Mapping.* 2008;29(7):802-809. doi:10.1002/hbm.20579
35. Kotlarz P, Nino JC, Febo M. Connectomic analysis of Alzheimer's disease using percolation theory. *Network Neuroscience.* 2022;6(1):213-233. doi:10.1162/netn_a_00221
36. Bero AW, Yan P, Roh JH, et al. Neuronal activity regulates the regional vulnerability to amyloid- β deposition. *Nat Neurosci.* 2011;14(6):750-756. doi:10.1038/nn.2801
37. Cirrito JR, Yamada KA, Finn MB, et al. Synaptic Activity Regulates Interstitial Fluid Amyloid- β Levels In Vivo. *Neuron.* 2005;48(6):913-922. doi:10.1016/j.neuron.2005.10.028
38. Bateman RJ, Xiong C, Benzinger TLS, et al. Clinical and Biomarker Changes in Dominantly Inherited Alzheimer's Disease. *New England Journal of Medicine.* 2012;367(9):795-804. doi:10.1056/NEJMoa1202753
39. Fabiani M, Gordon BA, Maclin EL, et al. Neurovascular coupling in normal aging: A combined optical, ERP and fMRI study. *NeuroImage.* 2014;85:592-607. doi:10.1016/j.neuroimage.2013.04.113
40. McKay NS, Gordon BA, Hornbeck RC, et al. Positron emission tomography and magnetic resonance imaging methods and datasets within the Dominantly Inherited Alzheimer Network (DIAN). *Nat Neurosci.* Published online July 10, 2023:1-12. doi:10.1038/s41593-023-01359-8
41. Strain JF, Brier MR, Tanenbaum A, et al. Covariance-based vs. Correlation-based Functional Connectivity Dissociates Healthy Aging from Alzheimer Disease. *NeuroImage.* Published online July 30, 2022:119511. doi:10.1016/j.neuroimage.2022.119511
42. Power JD, Mitra A, Laumann TO, Snyder AZ, Schlaggar BL, Petersen SE. Methods to detect, characterize, and remove motion artifact in resting state fMRI. *NeuroImage.* 2014;84:320-341. doi:10.1016/j.neuroimage.2013.08.048
43. White III RL, Campbell MC, Yang D, Shannon W, Snyder AZ, Perlmuter JS. Little Change in Functional Brain Networks Following Acute Levodopa in Drug-Naïve Parkinson's Disease. *Movement Disorders.* 2020;35(3):499-503. doi:10.1002/mds.27942

44. Behzadi Y, Restom K, Liau J, Liu TT. A component based noise correction method (CompCor) for BOLD and perfusion based fMRI. *NeuroImage*. 2007;37(1):90-101. doi:10.1016/j.neuroimage.2007.04.042
45. Raut RV, Mitra A, Snyder AZ, Raichle ME. On time delay estimation and sampling error in resting-state fMRI. *NeuroImage*. 2019;194:211-227. doi:10.1016/j.neuroimage.2019.03.020
46. Fischl B. FreeSurfer. *NeuroImage*. 2012;62(2):774-781. doi:10.1016/j.neuroimage.2012.01.021
47. Jenkinson M, Beckmann CF, Behrens TEJ, Woolrich MW, Smith SM. FSL. *NeuroImage*. 2012;62(2):782-790. doi:10.1016/j.neuroimage.2011.09.015
48. Wheelock MD, Strain JF, Mansfield P, et al. Brain network decoupling with increased serum neurofilament and reduced cognitive function in Alzheimer's disease. *Brain*. Published online January 10, 2023:awac498. doi:10.1093/brain/awac498
49. Power JD, Cohen AL, Nelson SM, et al. Functional Network Organization of the Human Brain. *Neuron*. 2011;72(4):665-678. doi:10.1016/j.neuron.2011.09.006
50. Seitzman BA, Gratton C, Marek S, et al. A set of functionally-defined brain regions with improved representation of the subcortex and cerebellum. *NeuroImage*. 2020;206:116290. doi:10.1016/j.neuroimage.2019.116290
51. Chen AA, Beer JC, Tustison NJ, et al. Mitigating site effects in covariance for machine learning in neuroimaging data. *Hum Brain Mapp*. 2022;43(4):1179-1195. doi:10.1002/hbm.25688
52. Rubinov M, Sporns O. Complex network measures of brain connectivity: Uses and interpretations. *NeuroImage*. 2010;52(3):1059-1069. doi:10.1016/j.neuroimage.2009.10.003
53. Rubinov M, Sporns O. Weight-conserving characterization of complex functional brain networks. *NeuroImage*. 2011;56(4):2068-2079. doi:10.1016/j.neuroimage.2011.03.069
54. Guimerà R, Nunes Amaral LA. Functional cartography of complex metabolic networks. *Nature*. 2005;433(7028):895-900. doi:10.1038/nature03288
55. Garrison KA, Scheinost D, Finn ES, Shen X, Constable RT. The (in)stability of functional brain network measures across thresholds. *Neuroimage*. 2015;118:651-661. doi:10.1016/j.neuroimage.2015.05.046
56. Drakesmith M, Caeyenberghs K, Dutt A, Lewis G, David AS, Jones DK. Overcoming the effects of false positives and threshold bias in graph theoretical analyses of neuroimaging data. *NeuroImage*. 2015;118:313-333. doi:10.1016/j.neuroimage.2015.05.011
57. Power JD, Schlaggar BL, Lessov-Schlaggar CN, Petersen SE. Evidence for Hubs in Human Functional Brain Networks. *Neuron*. 2013;79(4):798-813. doi:10.1016/j.neuron.2013.07.035

58. Brier MR, Thomas JB, Fagan AM, et al. Functional connectivity and graph theory in preclinical Alzheimer's disease. *Neurobiology of Aging*. 2014;35(4):757-768. doi:10.1016/j.neurobiolaging.2013.10.081
59. Hagmann P, Cammoun L, Gigandet X, et al. Mapping the Structural Core of Human Cerebral Cortex. *PLOS Biology*. 2008;6(7):e159. doi:10.1371/journal.pbio.0060159
60. Achard S, Delon-Martin C, Vértes PE, et al. Hubs of brain functional networks are radically reorganized in comatose patients. *Proc Natl Acad Sci USA*. 2012;109(50):20608-20613. doi:10.1073/pnas.1208933109
61. Song J, Nair VA, Gaggl W, Prabhakaran V. Disrupted Brain Functional Organization in Epilepsy Revealed by Graph Theory Analysis. *Brain Connectivity*. 2015;5(5):276-283. doi:10.1089/brain.2014.0308
62. Termenon M, Achard S, Jaillard A, Delon-Martin C. The "Hub Disruption Index," a Reliable Index Sensitive to the Brain Networks Reorganization. A Study of the Contralateral Hemisphere in Stroke. *Frontiers in Computational Neuroscience*. 2016;10. Accessed March 11, 2022. <https://www.frontiersin.org/article/10.3389/fncom.2016.00084>
63. Vatansever D, Schröter M, Adapa RM, Bullmore ET, Menon DK, Stamatakis EA. Reorganisation of Brain Hubs across Altered States of Consciousness. *Sci Rep*. 2020;10(1):3402. doi:10.1038/s41598-020-60258-1
64. Liang X, Zou Q, He Y, Yang Y. Coupling of functional connectivity and regional cerebral blood flow reveals a physiological basis for network hubs of the human brain. *Proceedings of the National Academy of Sciences*. 2013;110(5):1929-1934. doi:10.1073/pnas.1214900110
65. Sporns O, Honey CJ, Kötter R. Identification and Classification of Hubs in Brain Networks. *PLOS ONE*. 2007;2(10):e1049. doi:10.1371/journal.pone.0001049
66. Aschenbrenner AJ, James BD, McDade E, et al. Awareness of genetic risk in the Dominantly Inherited Alzheimer Network (DIAN). *Alzheimer's Dement*. 2020;16(1):219-228. doi:10.1002/alz.12010
67. Bateman RJ, Benzinger TL, Berry S, et al. The DIAN-TU Next Generation Alzheimer's prevention trial: Adaptive design and disease progression model. *Alzheimer's & Dementia*. 2017;13(1):8-19. doi:10.1016/j.jalz.2016.07.005
68. Wang G, Berry S, Xiong C, et al. A novel cognitive disease progression model for clinical trials in autosomal-dominant Alzheimer's disease. *Stat Med*. 2018;37(21):3047-3055. doi:10.1002/sim.7811
69. Brier MR, McCarthy JE, Benzinger TLS, et al. Local and distributed PiB accumulation associated with development of preclinical Alzheimer's disease. *Neurobiology of Aging*. 2016;38:104-111. doi:10.1016/j.neurobiolaging.2015.10.025
70. Su Y, D'Angelo GM, Vlassenko AG, et al. Quantitative Analysis of PiB-PET with FreeSurfer ROIs. *PLOS ONE*. 2013;8(11):e73377. doi:10.1371/journal.pone.0073377

71. Wisch JK, Roe CM, Babulal GM, et al. Resting State Functional Connectivity Signature Differentiates Cognitively Normal from Individuals Who Convert to Symptomatic Alzheimer Disease. *J Alzheimers Dis.* 2020;74(4):1085-1095. doi:10.3233/JAD-191039
72. Benjamini Y, Hochberg Y. Controlling the False Discovery Rate: A Practical and Powerful Approach to Multiple Testing. *Journal of the Royal Statistical Society: Series B (Methodological)*. 1995;57(1):289-300. doi:10.1111/j.2517-6161.1995.tb02031.x
73. Xia M, Wang J, He Y. BrainNet Viewer: A Network Visualization Tool for Human Brain Connectomics. *PLOS ONE*. 2013;8(7):e68910. doi:10.1371/journal.pone.0068910
74. Cole MW, Pathak S, Schneider W. Identifying the brain's most globally connected regions. *NeuroImage*. 2010;49(4):3132-3148. doi:10.1016/j.neuroimage.2009.11.001
75. Jack CR, Knopman DS, Jagust WJ, et al. Hypothetical model of dynamic biomarkers of the Alzheimer's pathological cascade. *The Lancet Neurology*. 2010;9(1):119-128. doi:10.1016/S1474-4422(09)70299-6
76. Sperling RA, Aisen PS, Beckett LA, et al. Toward defining the preclinical stages of Alzheimer's disease: Recommendations from the National Institute on Aging-Alzheimer's Association workgroups on diagnostic guidelines for Alzheimer's disease. *Alzheimer's & Dementia*. 2011;7(3):280-292. doi:10.1016/j.jalz.2011.03.003
77. Raj A, Kuceyeski A, Weiner M. A Network Diffusion Model of Disease Progression in Dementia. *Neuron*. 2012;73(6):1204-1215. doi:10.1016/j.neuron.2011.12.040
78. Detrez JR, Maurin H, Van Kolen K, et al. Regional vulnerability and spreading of hyperphosphorylated tau in seeded mouse brain. *Neurobiology of Disease*. 2019;127:398-409. doi:10.1016/j.nbd.2019.03.010
79. Mezias C, LoCastro E, Xia C, Raj A. Connectivity, not region-intrinsic properties, predicts regional vulnerability to progressive tau pathology in mouse models of disease. *acta neuropathol commun*. 2017;5(1):61. doi:10.1186/s40478-017-0459-z
80. de Reus MA, Heuvel MP van den. Rich Club Organization and Intermodule Communication in the Cat Connectome. *J Neurosci*. 2013;33(32):12929-12939. doi:10.1523/JNEUROSCI.1448-13.2013
81. Cao R, Wang X, Gao Y, et al. Abnormal Anatomical Rich-Club Organization and Structural-Functional Coupling in Mild Cognitive Impairment and Alzheimer's Disease. *Frontiers in Neurology*. 2020;11. Accessed September 25, 2023. <https://www.frontiersin.org/articles/10.3389/fneur.2020.00053>
82. Daianu M, Jahanshad N, Nir TM, et al. Rich club analysis in the Alzheimer's disease connectome reveals a relatively undisturbed structural core network. *Human Brain Mapping*. 2015;36(8):3087-3103. doi:10.1002/hbm.22830
83. Gratton C, Nomura EM, Pérez F, D'Esposito M. Focal Brain Lesions to Critical Locations Cause Widespread Disruption of the Modular Organization of the Brain. *J Cogn Neurosci*. 2012;24(6):1275-1285. doi:10.1162/jocn_a_00222

84. Mattson M, Cheng B, Davis D, Bryant K, Lieberburg I, Rydel R. beta-Amyloid peptides destabilize calcium homeostasis and render human cortical neurons vulnerable to excitotoxicity. *J Neurosci*. 1992;12(2):376-389. doi:10.1523/JNEUROSCI.12-02-00376.1992
85. Bezprozvanny I, Mattson MP. Neuronal calcium mishandling and the pathogenesis of Alzheimer's disease. *Trends in Neurosciences*. 2008;31(9):454-463. doi:10.1016/j.tins.2008.06.005
86. Hampel H, Hardy J, Blennow K, et al. The Amyloid- β Pathway in Alzheimer's Disease. *Mol Psychiatry*. 2021;26(10):5481-5503. doi:10.1038/s41380-021-01249-0
87. delEtoile J, Adeli H. Graph Theory and Brain Connectivity in Alzheimer's Disease. *Neuroscientist*. 2017;23(6):616-626. doi:10.1177/1073858417702621
88. Váša F, Mišić B. Null models in network neuroscience. *Nat Rev Neurosci*. 2022;23(8):493-504. doi:10.1038/s41583-022-00601-9
89. Fornito A, Zalesky A, Bassett DS, et al. Genetic Influences on Cost-Efficient Organization of Human Cortical Functional Networks. *J Neurosci*. 2011;31(9):3261-3270. doi:10.1523/JNEUROSCI.4858-10.2011
90. de Haan W, Straaten ECW van, Gouw AA, Stam CJ. Altering neuronal excitability to preserve network connectivity in a computational model of Alzheimer's disease. *PLOS Computational Biology*. 2017;13(9):e1005707. doi:10.1371/journal.pcbi.1005707
91. Tu W, Ma Z, Zhang N. Brain network reorganization after targeted attack at a hub region. *NeuroImage*. 2021;237:118219. doi:10.1016/j.neuroimage.2021.118219
92. Rubinov M, McIntosh AR, Valenzuela MJ, Breakspear M. Simulation of Neuronal Death and Network Recovery in a Computational Model of Distributed Cortical Activity. *The American Journal of Geriatric Psychiatry*. 2009;17(3):210-217. doi:10.1097/JGP.0b013e318187137a
93. Wepert DA, Lowe VJ, Knopman DS, et al. A robust biomarker of large-scale network failure in Alzheimer's disease. *Alzheimer's & Dementia: Diagnosis, Assessment & Disease Monitoring*. 2017;6:152-161. doi:10.1016/j.dadm.2017.01.004
94. Jones DT, Machulda MM, Vemuri P, et al. Age-related changes in the default mode network are more advanced in Alzheimer disease. *Neurology*. 2011;77(16):1524-1531. doi:10.1212/WNL.0b013e318233b33d
95. Wig GS. Segregated Systems of Human Brain Networks. *Trends in Cognitive Sciences*. 2017;21(12):981-996. doi:10.1016/j.tics.2017.09.006
96. Diez I, Sepulcre J. Unveiling the Neuroimaging-Genetic Intersections in the Human Brain. *Curr Opin Neurol*. 2021;34(4):480-487. doi:10.1097/WCO.0000000000000952
97. Wagstyl K, Sophie A, Jakob S, et al. Transcriptional Cartography Integrates Multiscale Biology of the Human Cortex. *eLife*. 2023;12. doi:10.7554/eLife.86933

Figure legends

Figure 1. Graph theory method and hub disruption. **(A)** A resting-state functional connectivity (FC) is obtained from the Pearson correlation of the time series in each of the 246 cortical and subcortical pre-defined region of interest (ROI) pairs. The ROIs belong to 13 Networks: SMd, somatomotor dorsal; SMI, somatomotor lateral; CO, cingulo-opercular; AUD, auditory; DMN, default mode network; Mem, memory network; Vis, visual network; FPN, frontoparietal network; SN, salience network; BG, basal ganglia; Thal, thalamus; VAN, ventral attention network; DAN, dorsal attention network. Following convention in previous literature, a sparse graph is generated by thresholding the rsFC matrix at an edge density threshold of 5% starting from the maximum spanning tree (MST) backbone to ensure the connectedness of the graph. However, to demonstrate that our results are not limited to the threshold choice we also applied other thresholds. The graph generated has weighted edges that preserve the strength of individual connections. **(B)** Original method of hub disruption calculation. **(C)** New method of hub disruption calculation. **(D)** Cartoon illustration of targeted attack at the hubs. **(E)** Cartoon illustrating random damage.

Figure 2. Functional connectivity (FC) within DIAN participant groups. Mean (lower-triangle) and standard deviation (upper-triangle) of Fisher Z-transformed FC matrix of 246 region of interests for mutation carriers (MC) at 3 Clinical Dementia Rating stages (CDR = 0, CDR = 0.5, CDR>=1) and corresponding age and EYO matched non-carrier (NC) groups. The FC is sorted by the networks in Figure 1 with corresponding colors.

Figure 3. Hub disruption across CDR stages. **(A)** (Left) Distribution of average strength (S) across NC match 1 group, (Middle) nodes with S higher than the 85th percentile. (Right) cartoon illustrating that strength is calculated by summing the weights across connected edges. **(B)** The % S difference against the baseline S Z-score in MC groups. **(C)** Individual hub disruption index (κ_S) for MC groups. **(D)** The % S difference against the baseline S Z-score in NC groups. **(E)** Individual κ_S for NC groups. **(F)** The % S difference against the baseline S Z-score in subsets of A β - and A β + participants in the MC(CDR=0) group. **(G)** Individual κ_S for A β - and A β + participants in the MC(CDR=0) group. Shaded areas show 95% confidence interval. Error bars show mean and standard deviation.

Figure 4. Hub disruption across CDR stages at module centers versus connectors. (A)

(Left) Distribution of average participation coefficient (Pc) across NC match 1 group, (Middle) distribution of within strength Z-score (Z) across NC match 1 group, (Right) cartoon illustrating the representation of module centers and connectors on a graph. Module centers are nodes with high Z and connectors are nodes with high Pc. **(B)** The % S difference against the baseline Pc Z-score for hub disruption calculation. **(C)** Individual hub disruption index (κ_S) for MC with respect to the group average Pc Z-score at NC match 1. **(D)** Individual hub disruption index (κ_S) for NC with respect to the group average Pc Z-score at NC match 1. **(E)** The % S difference against the baseline Z for hub disruption calculation. **(F)** Individual hub disruption index (κ_S) for MC with respect to the group average Z at NC match 1. **(G)** Individual hub disruption index (κ_S) for NC with respect to the group average Z at NC match 1. Lines show linear fit and shaded areas indicate the 95% CI.

Figure 5 Change in Biomarkers Across Estimated Years to Symptom Onset (EYO) for mutation carriers (MC) and non-carriers (NC). (A) The hub disruption index in strength (κ_S) against EYO, **(B)** The total cortical amyloid deposition measured with PiB against EYO, **(C)** The Cognitive Composite Score (CCS) against EYO. **(D)** The CCS against κ_S after regressing out potential confounding variables from both. The line and shaded areas show the predicted response values and the confidence intervals for the fitted responses from a generalized additive model at 95% interval calculated at each observation. For privacy reasons, the extreme EYO values (EYO<-20 and >10) were not displayed but were used in model-fitting.

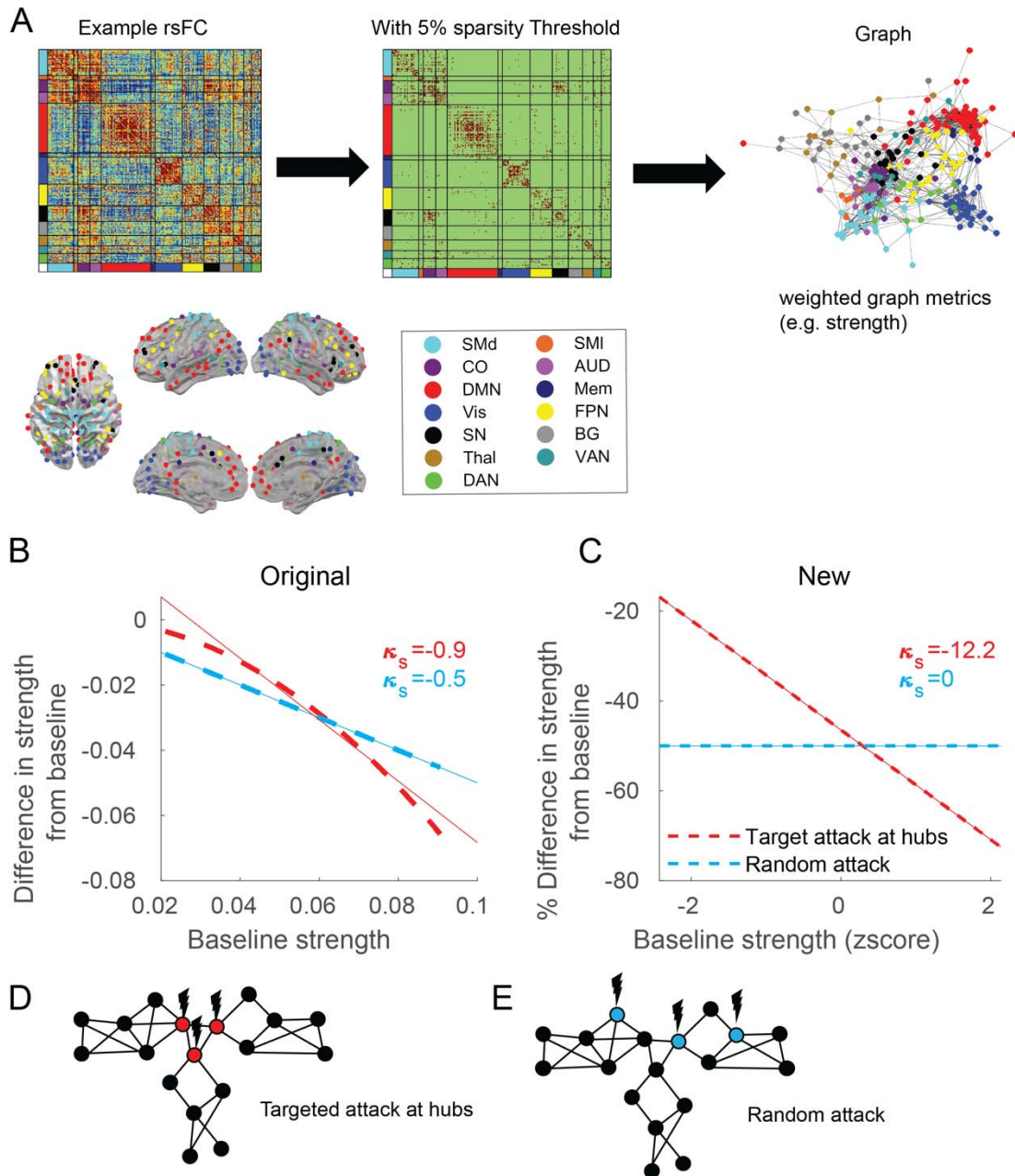


Figure 1

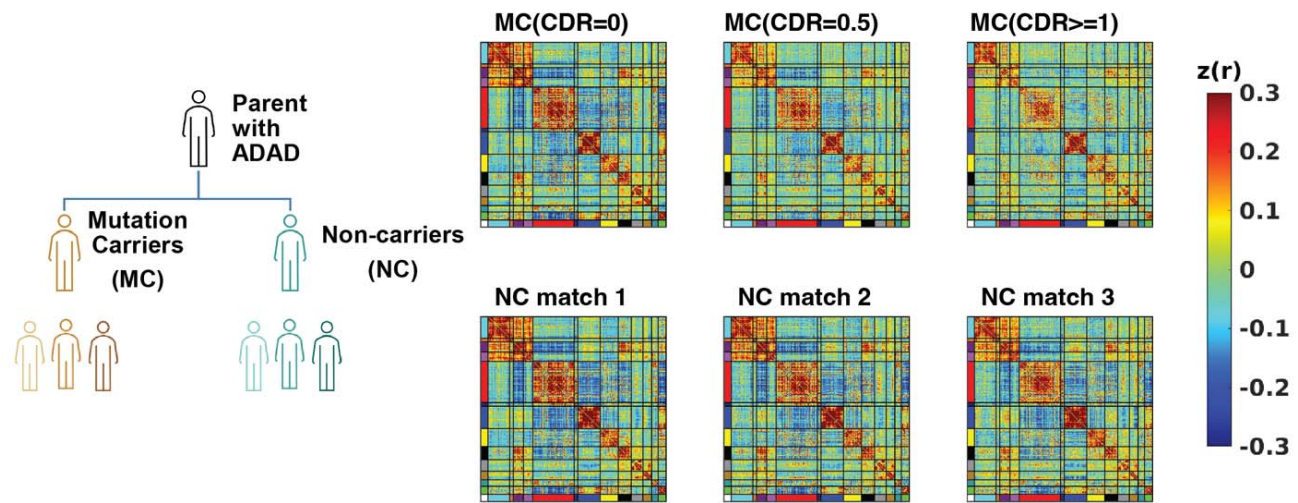


Figure 2

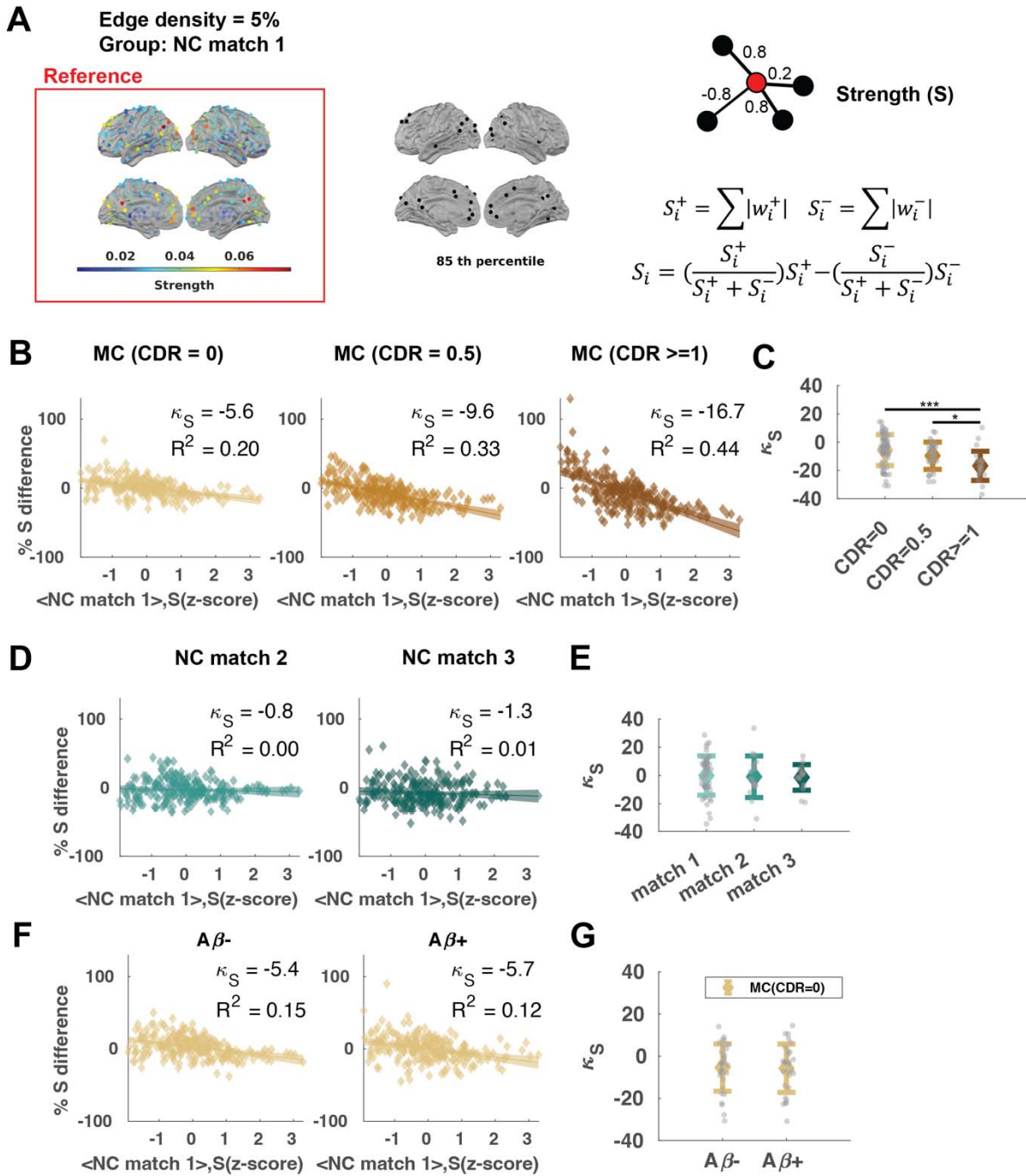


Figure 3

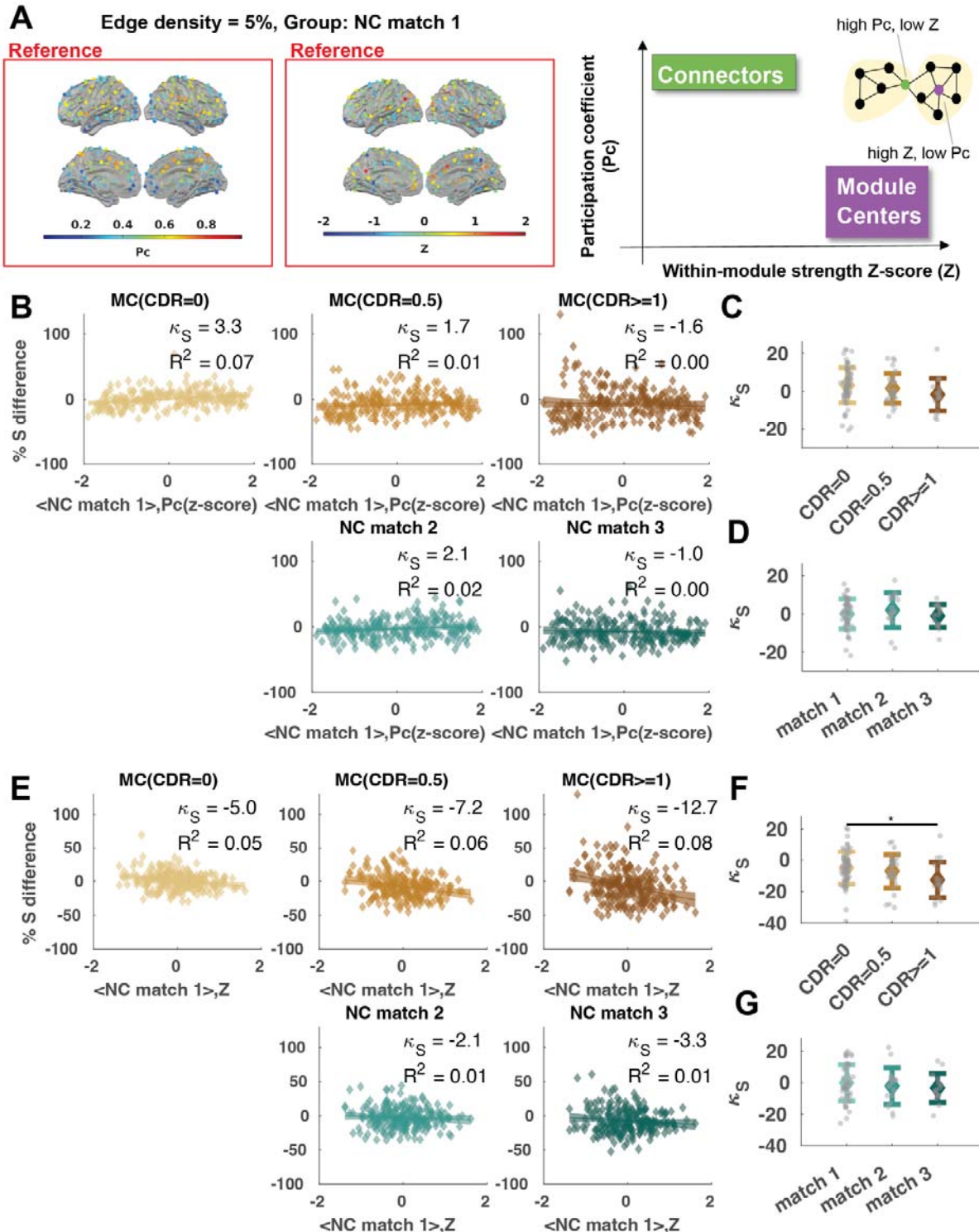


Figure 4

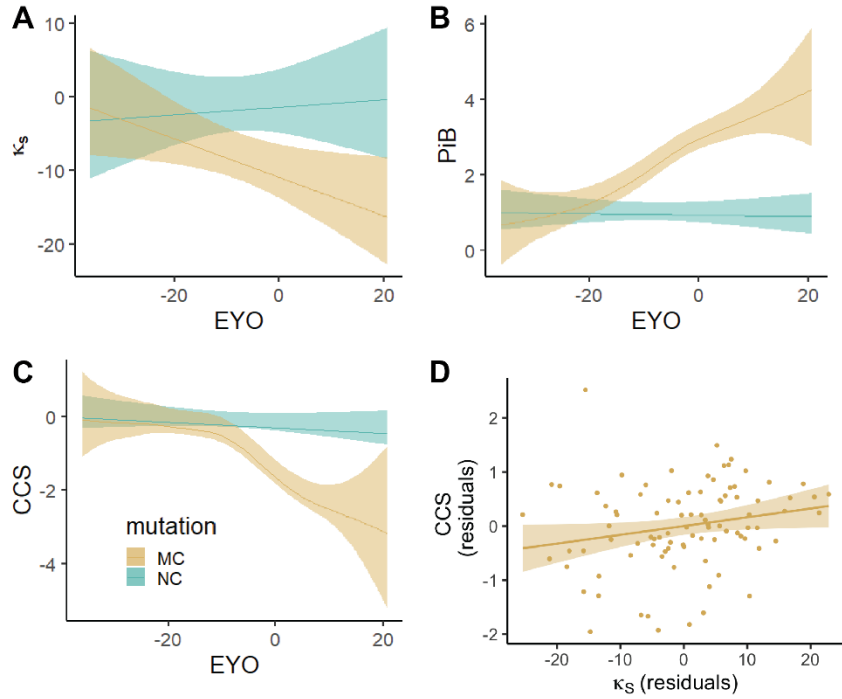


Figure 5

Table 1. Sample Characteristics (mutation carriers and non-carrier matches)

Table 1: Sample Characteristics (mutation carriers and non-carrier matches)						
	Measure	Mutation Carrier (N=69) ^a	Non-carrier match (N=52) ^b	Chi-Square	df	p-value
CDR=0/NC match 1	Sex (M/F)	36/33	23/29	0.749	1	0.387
	Family mutation (PS1, PS2, APP) n (%)	48 (70%), 11 (16%), 10 (14%)	36 (69%), 10 (19%), 6 (11%)	0.381	2	0.827
	APOE ε4 carriers/non-carriers	17/52	14/38	0.081	1	0.776
	Median			Mann-Whitney U	z	p-value
	Age (yrs)	33.2	34.4	1145	5.211	
	Education (yrs)	16	16	456.5	-3.487	0.956
	EYO	-15.1	-15.3	1244	6.456	0.563
	CCS ^c	-0.03	0.10	105	-5.702	0.116
	Remaining DVARS	5.1	4.8	1036	3.841	0.122
CDR=0.5/NC match 2	Remaining minutes of the scan	4.7	4.3	735	0.057	0.281
	Measure	Mutation Carrier (N=32)	Non-carrier match (N=17)	Chi-Square	df	p-value
	Sex (M/F)	13/19	3/14	2.666	1	0.103
	Family mutation (PS1, PS2, APP) n (%)	25 (78%), 1 (3%), 6 (19%)	8 (47%), 2 (12%), 7 (41%)	5.049	2	0.080
	APOE ε4 carriers/non-carriers	9/23	3/14	0.659	1	0.417
	median			Mann-Whitney U	z	p-value
	Age (yrs)	48.5	49.7	248.0	-0.504	
	Education (yrs)	13.5	14	205.5	-1.409	0.159
	EYO	1.7	1.7	235.0	-0.777	0.437
CDR ≥ 1/NC match 3	CCS ^d	-1.55	0.01	22.0	-5.159	<0.001
	Remaining DVARS	6.6	6.2	211.0	-1.281	0.200
	Remaining minutes of the scan	6.6	4.6	216.5	-1.166	0.243
	Measure	Mutation Carrier (N=20)	Non-carrier match (N=15)	Chi-Square	df	p-value
	Sex (M/F)	9/11	7/8	0.010	1	0.922
	Family mutation (PS1, PS2, APP) n (%)	17 (85%), 0 (0%), 3 (15%)	12 (80%), 3 (20%), 0 (0%)	6.276	2	0.043
	APOE ε4 carriers/non-carriers	5/15	5/10	0.292	1	0.589
	median			Mann-Whitney U	z	p-value
	Age (yrs)	50.8	55.4	131.0	-0.633	
a Removed 1 participant due to non-other participants existing from the same site b Removed 1 participant due to non-other participants existing from the same site c Missing 2 participant d Missing 2 participant e Missing 6 participant	Education (yrs)	12	14	82.5	-2.287	0.022
	EYO	4.3	4.9	138.0	-0.400	0.689
	CCS ^e	-2.71	-0.05	0.000	-4.583	<0.001
	Remaining DVARS	6.7	6.3	129.0	-0.700	0.484
	Remaining minutes of the scan	4.5	4.8	106.0	-1.468	0.142

Table 2. Group-level hub disruption (using metrics in NC match1 as baseline) across CDR stages in MC and across age in NC (FDR-adjusted).

Strength (S)					
	Group	κ_S	F (1,244)	p	R^2
MC	CDR = 0	-5.6	59.1	<0.001	0.20
	CDR = 0.5	-9.6	118.1	<0.001	0.33
	CDR>=1	-16.7	192.2	<0.001	0.44
NC	match 2	-0.8	0.78	0.38	0.003
	match 3	-1.3	1.46	0.28	0.006
Participation Coefficient (Pc)					
	Group	κ_S	F (1,244)	p	R^2
MC	CDR = 0	3.3	17.8	<0.001	0.07
	CDR = 0.5	1.7	2.5	0.19	0.01
	CDR>=1	-1.6	1.0	0.34	0.44
NC	match 2	2.1	4.7	0.08	0.02
	match 3	-1.0	0.9	0.34	0.003
Within-module Strength Z-score (Z)					
	Group	κ_S	F (1,244)	p	R^2
MC	CDR = 0	-5.0	12.6	<0.001	0.05
	CDR = 0.5	-7.2	15.5	<0.001	0.06
	CDR>=1	-12.7	22.1	<0.001	0.08
NC	match 2	-2.1	1.6	0.21	0.01
	match 3	-3.3	2.9	0.11	0.01

Table 3. Regression of hub disruption index on Cognitive Composite Score (CCS). Response: Cognitive Composite Scores (CCS). β , coefficient of regression. ***p<0.001, **p<0.01, *p<0.05. Random effect: family.

Edge threshold	β_{kS}	$\beta_{\text{Education}}$	β_{Age}	$\beta_{\text{Sex (Male)}}$	β_{DVARS}
5%	0.02*	0.11***	-0.06***	-0.18	-0.04
10%	0.03**	0.11***	-0.06***	-0.18	-0.05
20%	0.05**	0.11***	-0.06***	-0.19	-0.06
30%	0.07**	0.11***	-0.06***	-0.20	-0.07
40%	0.09**	0.10***	-0.06***	-0.21	-0.07